Journal of Physics: Conference Series **2894** (2024) 012025 doi:10.1088/1742-6596/2894/1/012025

Photon Vortex Production from Synchrotron Radiation of Electron in Relativistic Quantum Approach

Tomoyuki Maruyama

College of Bioresource Sciences, Nihon University, Fujisawa 252-0880, Japan

E-mail: maruyama.tomoyuki@nihon-u.ac.jp

Takehito Hayakawa

National Institutes for Quantum and Radiological Science and Technology, Tokai, Ibaraki 319,-1106, Japan

Toshitaka Kajino

Beihang University, School of Physics, International Research Center for Big-Bang Cosmology and Element Genesis, Beijing 100083, China

Myung-Ki Cheoun

Department of Physics, Soongsil University, Seoul 156-743, Korea

Abstract. Light vortices exhibit a remarkable feature: a single photon can harbor a vortex wave-function on the quantum scale. In this study, we illustrate the process behind creating a photon vortex using a Bessel wave-function. Furthermore, we calculate the decay widths stemming from an electron in Landau levels and the energy spectra of photons emitted with a non-zero orbital angular momentum along their propagation direction. The results suggest the possible presence of photon vortices in astrophysical environments distinguished by strong magnetic fields.

Light vortices, bearing substantial angular momenta [1], captivate interest for both fundamental physics exploration and practical applications. The discourse on the emergence of light vortices within the cosmos has also found resonance [2, 3, 4]. Notably, proposals have surfaced suggesting the potential creation of photon vortices in the vicinity of rotating black holes [4]. An intriguing aspect of light vortices lies in the possibility that a solitary photon can harbor a vortex wave-function at the quantum level [1]. This photon vortex holds promise for the quantum manipulation of materials, including atoms [5], molecules [6], and nuclei [7], as well as for advancements in quantum communications [8]. The foundational processes involved in photon production, such as harmonic radiations from a spiral-moving electron under magnetic fields [9, 10] and nonlinear inverse Compton scattering with highly intense circularly polarized lasers [11], emerge as viable candidates for efficient photon vortex production. This is attributed to the fact that, in these processes, a single electron emits a photon. Despite the

demonstrated production of light vortices using helical undulators [12, 13, 14], these procedures remain underexplored within the realm of quantum mechanics.

Recently, the phase structure of harmonic radiations from spiral-moving electrons under magnetic fields was computed within classical electromagnetism [9]. The findings suggest that an m-th harmonic photon serves as a photon vortex carrying $m\hbar$ total angular momentum. However, the question of whether each individual photon possesses the wave-function of a photon vortex remains unresolved at the quantum level.

This work builds upon the analysis and results presented in [15], where I discussed related findings during my conference talk; further details can be found in that paper.

In quantum mechanics, electron orbitals under magnetic fields undergo Landau quantization. When a moving electron in a magnetic field loses energy through a transition associated with photon emission, its initial and final states correspond to the eigen-states in Landau quantization. Landau quantization plays a crucial role in various phenomena, such as terahertz nonlinear optics. Furthermore, under strong magnetic fields, Landau quantization may yield results significantly different from those based on classical electron behavior [15, 16, 17]. In this study, we present evidence that the photon generated by harmonic radiations from a spiral-moving electron under a uniform magnetic field is a photon vortex with a Bessel wave-function in quantum mechanics [18].

We employ natural units where $\hbar = c = 1$ and consider a uniform dipole magnetic field directed along the z-axis, represented as $\boldsymbol{B} = (0, 0, B)$. The symmetry gauge is chosen with the vector potential defined as $\boldsymbol{A} = B(-y, x, 0)/2$.

The electron wave function $\psi(\boldsymbol{r})$ in this system is derived from the following Dirac equation:

$$\left[\boldsymbol{\alpha} \cdot (-i\boldsymbol{\nabla}_r + e\boldsymbol{A}) + \beta m_e\right] \psi(\boldsymbol{r}) = E\psi(\boldsymbol{r}), \tag{1}$$

where m_e is the mass of the electron. The wave function of the electron, as a solution to this Dirac equation, can be expressed as an eigenstate of the z-component of the total angular momentum (zTAM), J, and the z-component of momentum, p_z:

$$\begin{aligned}\psi(\boldsymbol{r}) &= \left\{ \frac{1+\Sigma_z}{2} G^{n'}_{L-1}\left(\sqrt{\frac{eB}{2}}\boldsymbol{r}_T\right) + \frac{1-\Sigma_z}{2} G^{n}_{L}\left(\sqrt{\frac{eB}{2}}\boldsymbol{r}_T\right)\right\} \\ &\quad \times \frac{E+m_e}{2E}\begin{bmatrix} \chi_s \\ \frac{1}{E+m_e}\left(p_z\sigma_z + \sqrt{2eBN_L}\sigma_y\right)\chi_s, \end{bmatrix} \frac{e^{ip_z z}}{\sqrt{R_z}},\end{aligned} \tag{2}$$

where $G^n_L(\boldsymbol{r}_T)$ denotes the two-dimensional harmonic oscillator wave function, and the spatial coordinate is expressed as $\boldsymbol{r} = (\boldsymbol{r}_T, z) = (r_T \cos\phi_r, r_T \sin\phi_r)$. Here, R_z represents the size of the system along the z-direction, χ_s is the Pauli spinor, $\Sigma_z = \mathrm{diag}(1, -1, 1, -1)$, and L is the z-component of the orbital angular momentum (zOAM), satisfying the relationship $J = L + s/2$. The parameter n represents the number of nodes in the amplitude of the wave function along the radial direction in the xy-plane, with $n' = n$ when $L \geq 0$ and $n' = n - 1$ when $L \leq -1$. The Landau level number is defined as $N_L = (L + |L|)/2 + n$. The energy of the electron in Landau levels is given by: $E = \sqrt{2eBN_L + p_z^2 + m_e^2}$.

We consider photon emission resulting from an electron transitioning between two Landau levels. The initial and final electron states correspond to eigenstates of zTAM, J_i and J_f, respectively. Consequently, the photon state is characterized as an eigenstate of its zTAM, $K = J_i - J_f$, and the z-component of momentum, q_z, known as the Bessel wave.

By utilizing the Coulomb gauge with $\boldsymbol{\nabla} \cdot \boldsymbol{A} = 0$ and $A_0 = 0$, we derive the two orthogonal wave functions for the Bessel wave as follows:

$$\boldsymbol{A}^{(TM)}_K = \frac{1}{2e_q} e^{i(q_z z - e_q t)} \left[iq_z\left(\tilde{J}_{K+1} - \tilde{J}_{K-1}\right), q_z\left(\tilde{J}_{K+1} + \tilde{J}_{K-1}\right), 2q_T\tilde{J}_K \right], \tag{3}$$

$$\boldsymbol{A}_K^{(TE)} = \frac{1}{2} e^{i(q_z z - e_q t)} \left[i\left(\tilde{J}_{K+1} + \tilde{J}_{K-1}\right), \left(\tilde{J}_{K+1} - \tilde{J}_{K-1}\right), 0 \right] \tag{4}$$

where $\tilde{J}_L(\boldsymbol{r}_T) = J_L(q_T r_T) e^{iL\phi}$ with $q_T = \sqrt{e_q^2 - q_z^2}$, and J_L representing the Bessel function. The transition with $K = 1$ corresponds to fundamental radiation, while transitions with $K \geq 2$ exhibit helical vortex structures as harmonic radiations. This indicates that a spiraling electron, subjected to a uniform strong magnetic field, emits a photon vortex with a non-zero zTOM at the quantum level.

The wave function in Eq. (2) for $n = 0$ and $L \geq 0$ corresponds to helical motion along the z-axis, whereas wave functions for other cases are superpositions of electron states for helical motions along axes distinct from the initial axis [19]. For our purposes, we select $n_i = 0$ and $Li \geq 0$ for the initial state. Furthermore, we consider only $n_f = 0$ for the final electron states in this study. In practical calculations, the decay widths to final electron states with $n_f = 0$ dominate in the low K region, and this restriction poses no significant issues.

The decay width of an electron is computed as the imaginary part of the electron self-energy derived from the initial and final wave functions. The decay width for the electron in state i is given by:

$$\Gamma_e(i) = \frac{e^2}{8\pi^2} \sum_{f,K,\alpha} \int dq_z \left| \int d\boldsymbol{r}_T \overline{\psi}_f(\boldsymbol{r}) \not{A}_K^{(\alpha)*}(\boldsymbol{r}) \psi_i(\boldsymbol{r}) \right|^2, \tag{5}$$

where the subscript f denotes the final electron state.

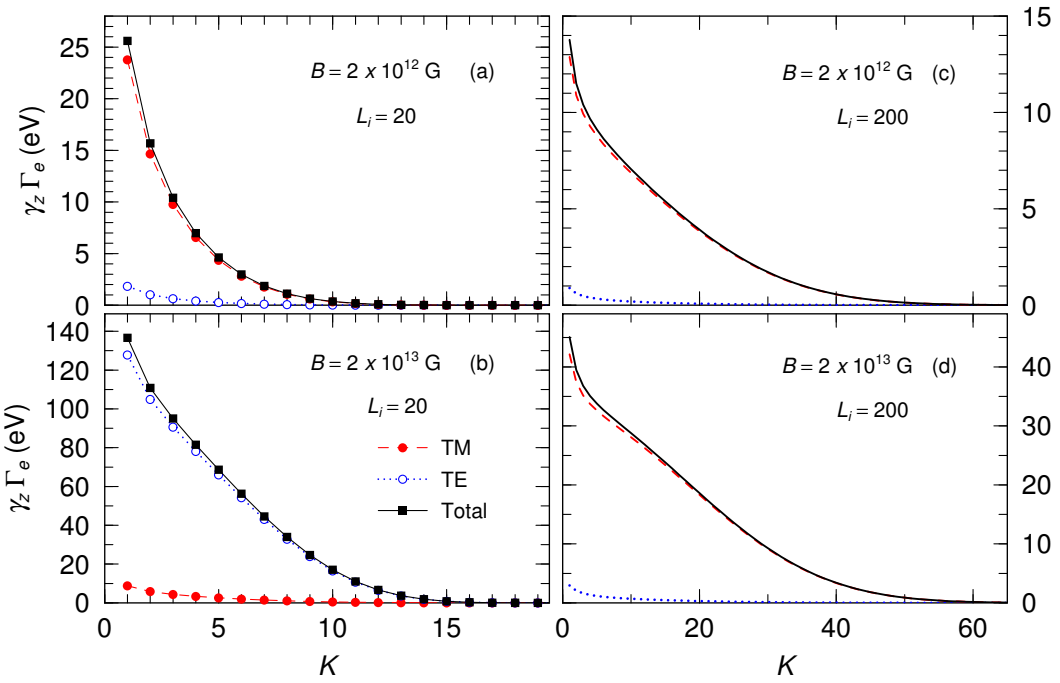

Figure 1. Decay widths of electrons as a function of zTAM of an emitted photon, with the final electron's Landau level fixed. Results are shown for magnetic field strengths of 2×10^{12} G in the upper panels (a, c) and 2×10^{13} G in the lower panels (b, d), with initial orbital angular momenta $L_i = 20$ in the left panels (a, b) and $L_i = 200$ in the right panels (c, d). The dashed and dotted lines represent the photon field in TM and TE modes, respectively, while the solid line shows the sum of both contributions

To elucidate the quantum effects clearly, we numerically calculate the decay widths for electrons under strong magnetic fields, such as 2×10^{12} G and 2×10^{13} G, which are commonly found in astrophysical objects, as discussed later.

Figure 1 shows the decay widths of electrons as a function of K in strong magnetic fields of 2×10^{12} G (a, c) and 2×10^{13} G (b, d). with initial orbital angular momenta $L_i = 20$ (a, b) and $L_i = 200$ (c, d). These results are factorized with the gamma factor in the z-direction, which is given by $\gamma_z = E_i/\sqrt{2eBL_i + m_e^2}$, and they do not depend on the z-component of the initial electron momentum p_{iz} as confirmed by numerical testing for the condition $|p_{iz}| \gg m_e$

The decay widths change with the magnetic field strength. As the strength increases, all modes show larger decay widths, and the amount of high-order harmonic radiation also rises. In addition, the fraction of decay widths for $K \geq 2$ increases when the initial electron angular momentum becomes larger, which is connected to the size of the electron's spiral motion. This dependence on magnetic field strength is, however, more apparent when $Li = 20$, while it becomes less noticeable when $L_i = 200$, indicating that the magnetic field effect is clearer at lower initial angular momentum.

Circular polarization is related to helicity. As mentioned before, the wave function of an emitted photon corresponds to either the TM-mode or TE-mode. The fact that the TM-mode appears in all cases means that the radiation is either unpolarized or has only a small amount of circular polarization. This happens because the photon momentum is not aligned with the direction of vortex propagation. As the angle between the momentum and the vortex direction gets smaller, the amount of TE-mode increases. When they become parallel, the photon has helicity of $h = +1$, meaning circular polarization, but it loses its vortex structure [15].

Figure 2 shows the energy spectrum of radiative photons, integrated over all emission angles, for magnetic fields of 10^{12} G (a, b) and 10^{13} G (c, d). The spectra are calculated for initial electron energies of 20 MeV (a, c) and 200 MeV (b, d). The possible energy of an emitted photon with K is limited by

$$\frac{eBK}{E_i + p_{iz}} \leq e_q \leq \frac{eBK}{E_i - p_{iz}}. \tag{6}$$

The maximum (or minimum) photon energy depends on K. So, at high energies, photon vortices with large angular momenta are produced.

The overall behavior in all four cases is similar. ¡ As the magnetic field strength gets stronger, both the decay width and the emitted photon energy increase. Also, when the incident energy rises by a factor of ten, from 20 MeV to 200 MeV, the decay width drops by a factor of one hundred, and the photon energy increases by a factor of ten. The integrated values also decrease by a factor of ten as the incident energy increases. These results follow the scaling by the relativistic gamma factor γ_z, as explained in Fig. 1.

In summary, this study focuses on how photon vortices are produced when electrons in Landau levels emit radiation in a magnetic field. We used the exact wavefunction, including Landau quantization, to describe the electron's motion accurately. Our results show that the m-th harmonic photon, caused by harmonic radiation from the electron's spiral motion in a uniform magnetic field, has a Bessel wave feature and carries a z-component of total angular momentum (zTAM) of $K = m + 1$. These photon vortices are likely to form in astrophysical environments with strong magnetic fields between 10^{12} and 10^{13} G. While the emitted photons don't have a coherent structure, they might act like white light and could be detected by future satellite-based detectors using Compton scattering.

Photonuclear reactions with photon vortices are affected by angular momentum conservation, which influences the isotopic makeup of nuclides created in these high-magnetic-field environments.

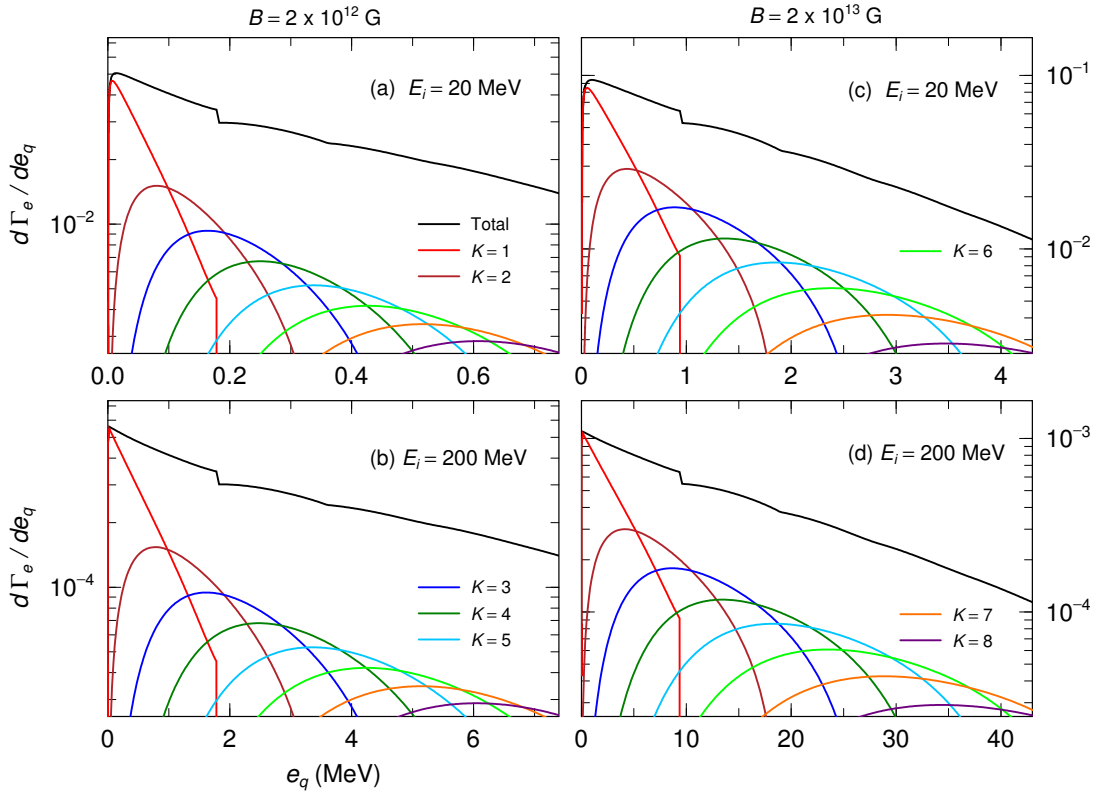

Figure 2. $d\Gamma_e/cde_q$ as a function of the photon energy e_q with $L_i = 20$. Results are shown for magnetic field strengths of 10^{12} G in the left panels (a, b) and 10^{13} G in the right panels (c, d) with incident energies of 20 MeV in the upper panels (a, c) and 200 MeV in the lower panels,(b, d).

Polarized γ-rays from γ-ray bursts (GRBs) have already been seen by satellite detectors [21, 22, 20]. Synchrotron radiation in strong magnetic fields is thought to be a possible source of these polarized photons [23]. This study clearly shows that photon vortices can be produced in various astrophysical settings with strong magnetic fields. Photon vortices are expected to be common in magnetic fields as strong as 10^{13} G, like those in magnetars [24] and magnetized accretion disks around black holes [25]. Although photon vortices from higher-order harmonic radiation are almost unpolarized, making it hard to detect them through polarization measurements, a method for detecting Laguerre-Gaussian (LG) light from astrophysical sources at optical wavelengths has been suggested [3]. This could make it possible to detect Bessel wave photons in a similar way, especially for LG γ-rays with energies above several tens of keV using Compton scattering [26, 27].

Finally, we briefly mention how these phenomena can be tested experimentally. In most experiments, magnetic fields are limited to about 10T ($= 10^5$G), which gives electrons a Larmor radius of about 10µm. While calculating the zOAM value is simple, it becomes difficult to integrate Eq.(5) when the zOAM is very large, around $L_i \approx 7.6 \times 10^5$. To handle this, we developed an approximate method. Additionally, an approximation for the integration in Eq. (7) can be used when $n_i = n_f = 0$ and $L_i \gg 1$, as explained in Ref. [28].

Acknowledgments
This work was supported by Grants-in-Aid for Scientific Research of JSPS (JP20K03958, JP19K03833, JP18H03715) and the grant of Joint Research by the National Institutes of Natural Sciences (NINS), (NINS program No, 01111701). MKC work was supported by the National Research Foundation of Korea (Grant Nos. NRF-2020R1A2C3006177 and NRF-2013M7A1A1075764).

[1] L. Allen, M. W. Beijersbergen, R. J. C. Spreeuw, and J. P. Woerdman, *Phys. Rev.* A **45**, 8185 (1992).
[2] N. M. Elias II, *Astronom. Astrophys.* **492**, 883 (2008).
[3] G. C. G. Berkhout and M. W. Beijersbergen, *Phys. Rev. Lett.* **101**, 100801 (2008).
[4] F. Tamburini, B. Thidé, G. Molina-Terriza, and G. Anzolin, Nature Phys. **7**, 195 (2011).
[5] A. Afanasev, C. E. Carlson, and A. Mukherjee, *Phys. Rev.* A. **88** 033841 (2013).
[6] A. Alexandrescu, D. Cojoc, and E. I. DiFabrizio, *Phys. Rev. Lett.* **96**, 243001 (2006).
[7] A. Afanasev, V. S. Serbo, and M. Solyanik, J. Phys. G. Nucl. Part. Phys. **45**, 055102 (2017).
[8] E. V. Kovlakov, I. B. Bobrov, S. S. Straupe, and S. P. Kulik, *Phys. Rev. Lett.* **118**, 030503 (2017).
[9] M. Katoh, M. Fujimoto, H. Kawaguchi, K. Tsuchiya, K. Ohmi, T. Kaneyasu, Y. Taira, M. Hosaka, A. Mochihashi, and Y. Takashima, *Phys. Rev. Lett.* **118**, 094801 (2017).
[10] S. Sasaki and I. McNulty, *Phys. Rev. Lett.* **100**, 124801 (2008).
[11] Y. Taira, T. Hayakawa, and M. Katoh, Sci. Rep. **7**, 5018 (2017).
[12] J. Bahrdt, K. Holldack, P. Kuske, R. Müller, M. Scheer, and P. Schmid, *Phys. Rev. Lett.* **111**, 034801 (2013)
[13] T. Kaneyasu, Y. Hikosaka, M. Fujimoto, T. Konomi, M Katoh, H Iwayama, and E. Shigemasa, *Phys. Rev.* A **95**, 023413 (2017) .
[14] E. Hemsing, A. Knyazik, M. Dunning, D. Xiang, A. Marinelli, C. Hast, and J. B. Rosenzweig, *Nature Phys.* **9**, 549 (2013).
[15] T. Maruyama, T. Hayakawa, T. Kajino and M.-K. Cheoun, *Phys. Lett.* B **826**. 136779 (2022)
[16] K. Hattri and K. Itakura, Ann. Phys. **334**, 58 (2013); K. Hattri and K. Itakura, Ann. Phys. **348**, 364 (2014).
[17] T. Maruyama, M. -K. Cheoun, T. Kajino, and G. J. Mathews, Phys. Lett. B **75**, 125 (2016).
[18] M. Kachelriess, C. Wilke, and G. Wunner, *Phys. Rev.* D **56**, 1313 (1997).
[19] R. Kubo, S. J. Miyake, and N. Hashitsume, *Solid State Phys.* **17**, 269 (1965).
[20] K. Wiresema, et al., *Nature* **509**, 201 (2014).
[21] E. Kalemci, S. E. Boggs, C. Kouveliotou, M. Finger, and M. G. Baring, *Astrophys. J. Supp.* **169**, 75 (2007).
[22] D. Yonetoku, T. Murakami, S. Gunji, T. Mihara, K. Toma, Y. Morihara, T. Takahashi, Y. Wakashima, H. Yonemochi, T. Sakashita, N. Toukairin, H. Fujimoto, and Y. Kodama, *Astrophys. J. Lett.* **758**, L1 (2012).
[23] A. Panaitescu and P. Mészáros, *Astrophys. J. Lett.* **544**, L17 (2000).
[24] S. Mereghetti, *Annu. Rev. Astrophysm.* **15**, 225 (2008).
[25] J.C. McKinney, A. Tchekhovskoy, and R.D. Blandford, Science **39**, 49 (2013).
[26] T. Maruyama, T. Hayakawa, and T. Kajino, Sci. Rep. **9**, 51 (2019).
[27] T. Maruyama, T. Hayakawa, and T. Kajino, Sci. Rep. **9**, 7998 (2019).
[28] T. Maruyama, T. Hayakawa, R. Hajima, T. Kajino, and M,-K. Cheoun, *Phys. Rev. Res.* **5**, 043289 (2023),